Influence of Site Effects on Observed Ground Motions in the Wellington Region from the $M_{\rm w}$ 7.8 Kaikōura, New Zealand, Earthquake

by Brendon A. Bradley, Liam M. Wotherspoon, Anna E. Kaiser, Brady R. Cox, and Seokho Jeong

Abstract This article presents ground-motion and site-effect observations in the Wellington region of New Zealand from the 14 November 2016 $M_{\rm w}$ 7.8 Kaikōura earthquake. Despite being ~60 km from the northern extent of the causative earthquake rupture, amplification of long-period ground motions due to site and basin-edge effects resulted in appreciable ground motions and subsequent damage to the built environment in this major urban area and capital city of New Zealand. The largest long-period ground motions were observed in the Thorndon and Te Aro basins in central Wellington, where similar site amplification effects were also observed during the 2013 Cook Strait earthquake sequence. Comparisons of pseudoacceleration response spectra with current estimates of fundamental site period across central Wellington indicate that this long-period amplification, relative to nearby rock stations, cannot be explained by 1D site effects alone (i.e., layered impedance), and thus it is inferred that there is a significant contribution from basin-edge-generated surface waves. In contrast, in the Lower Hutt-Petone area, north of central Wellington, ground motions from the GeoNet strong-motion station array across a deep alluvial valley clearly demonstrate the influence of 1D site effects. The 5%–95% significant duration of ground motions in central Wellington was on the order of 30 s, consistent with empirical models for this earthquake magnitude and source-to-site distance. The observations from the 2016 Kaikōura earthquake and comparison with the groundmotion characteristics of recent earthquakes has highlighted the need to improve characterization of the regional basin structures, particularly in regard to quantifying the contribution of basin resonance and basin-edge-generated surface waves.

Introduction

The $M_{\rm w}$ 7.8 Kaikōura earthquake struck the northeastern region of the South Island of New Zealand on 14 November 2016 at 12.02 a.m. local time (Kaiser, Balfour, et al., 2017). The epicenter was located in a rural region \sim 4 km from the small town of Waiau in north Canterbury. The earthquake source involved complex rupture of a number of faults, several of which were previously identified and several of which were not known to be active (Hamling et al., 2017; Stirling et al., 2017). Although the epicenter was \sim 200 km from Wellington, the capital city of New Zealand, the rupture propagated toward the northeast over a distance of \sim 150 km (Kaiser, Balfour, et al., 2017), such that the Wellington region was located only 60 km north of the northernmost surface fault rupture.

In general, the Wellington region experienced moderate ground motions relative to seismic design levels; however, in some locations in central Wellington the 500-yr return-period design ground motions were exceeded in the 1–2 s vibration period range (Bradley, Razafindrakoto, and Polak, 2017).

This placed significant demands on concrete moment frame buildings of 5–15 stories (mid-rise), leading to varying degrees of beam hinging, beam elongation, and damage to floors diaphragms (Henry *et al.*, 2017). There was also extensive nonstructural damage to a wider range of building typologies (Baird and Ferner, 2017). As a result, a number of buildings were demolished and a targeted assessment program was undertaken by local authorities to identify the extent of potentially affected buildings (Brunsdon *et al.*, 2017). Severe liquefaction-induced damage was evident across the port facilities on deep reclamation along the Wellington waterfront (Cubrinovski *et al.*, 2017), whereas outside this area only minor liquefaction-induced damage was evident in the other reclaimed areas (Orense *et al.*, 2017).

The Wellington region was also subjected to moderate intensity ground motions during two earthquakes in 2013, which occurred in the region close to the northern extent of the Kaikōura rupture (Fig. 1a). The 21 July 2013 $M_{\rm w}$ 6.6 Cook Strait (also referred to as Seddon) earthquake had

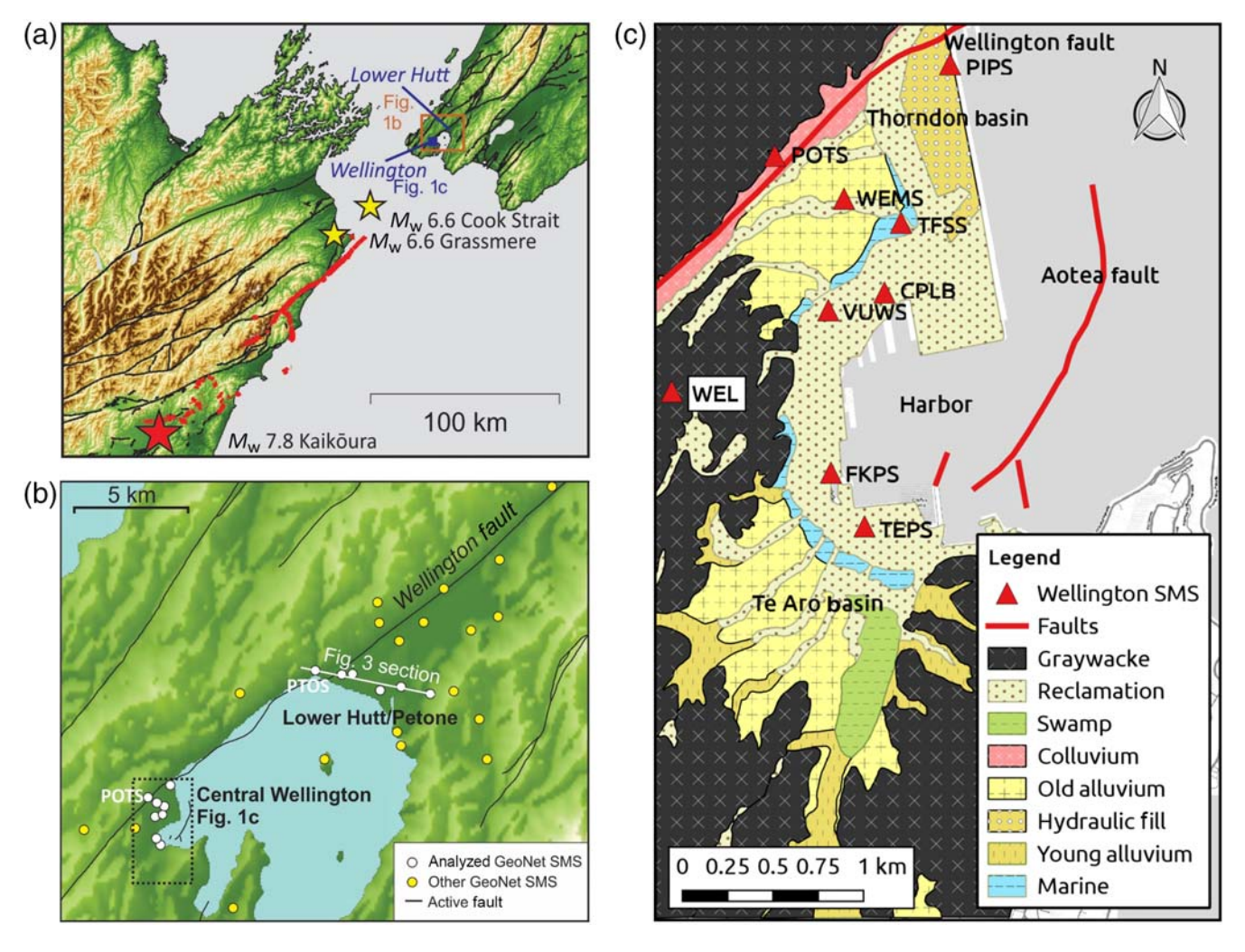


Figure 1. (a) Overview of the central region of New Zealand, showing the location of Wellington and Lower Hutt and major regional earthquakes since 2013 (epicenters shown as stars). The mapped surface fault ruptures of the Kaikōura earthquake are shown as thick lines (after Hamling *et al.*, 2017; Kaiser, Balfour, *et al.*, 2017) and other active faults are shown as thin lines (after Langridge *et al.*, 2016). Location of maps shown in (b,c) are also illustrated; (b) Lower Hutt and Wellington region, showing the location of strong-motion stations (SMSs), indicated by circular symbols. Location of maps in (c) and Figure 3 are also illustrated; (c) location of central Wellington SMSs, indicated by triangle symbols, against the backdrop of surface geologic characteristics (based on Semmens *et al.*, 2010). Locations of known active faults and the Te Aro and Thorndon basins are presented here. The color version of this figure is available only in the electronic edition.

an epicenter \sim 50 km southwest of Wellington, whereas the 16 August 2013 $M_{\rm w}$ 6.6 Lake Grassmere earthquake was located \sim 70 km southwest of Wellington. Of these two events, the highest intensity ground motions in Wellington were experienced in the Cook Strait earthquake, with over 30 buildings experiencing damage in central Wellington, and minor liquefaction and damage to the port facilities in Wellington (Holden *et al.*, 2013).

This article presents the features of the observed ground motions in the Wellington region during the Kaikōura earthquake, with comparison to the prior 2013 earthquakes, and a focus on the influence of seismic site effects in sedimentary soils. To provide context, the geotechnical and geologic setting of the region and the historic reclamation along the Wellington waterfront are first discussed. The site characteristics across the network of strong-motion stations (SMSs) in

the region are then presented in relation to this setting, drawing on the outcomes of recent field investigation at these locations. The characteristics and spatial distribution of shaking intensity are then discussed in relation to local site amplification, the influence of basin and basin-edgegenerated surface waves, and the significant duration.

Geotechnical and Geologic Setting

The geologically active Wellington region is located at the southern end of the North Island of New Zealand (Fig. 1). The active tectonic and geomorphological processes in the region resulted in complex and varied geological and geotechnical conditions. A number of major seismogenic sources are present in the region, including the Wellington fault, located along the edge of the two focus areas in this region of central Wellington and Lower Hutt–Petone.

Basement rock under central Wellington comprises graywacke, Permian to early Jurassic quartzo-feldspathic sandstone and mudstone sequences (Begg and Mazengarb, 1996). The maximum confirmed depth to basement under central Wellington is 137 m, with greater depths to bedrock expected in other areas based on geologic and geophysical evidence (Semmens et al., 2010). Graywacke basement outcrops in the hills surrounding central Wellington, and there are significant differences in weathering, sedimentological, and structural characteristics within this unit (Semmens et al., 2010).

Pleistocene deposits lie unconformably on the bedrock and consist of weathered alluvium, colluvium, and marine deposits composed of silty sandy gravels, interbedded with stiff silts and organic clays. Figure 1c illustrates that the complex surficial geology in central Wellington (Semmens et al., 2010) comprises bedrock in the surrounding hills, Pleistocene deposits, Holocene sediments, and reclamation deposits. Outside of the areas of reclamation, the Holocene deposits consist of weathered alluvium and colluvium, beach, estuarine, and swamp deposits.

Over 155 ha have been reclaimed along the central Wellington waterfront since 1852 (Kelly, 2005). The main types of material used in this process were hydraulic fill, consisting of pumped sand and mud from the seabed, and locally sourced end-tipped quarried rock. Reclamations of up to 17 m thickness are present and overlie thin Holocene beach and marine sediments and Pleistocene deposits. The most recent reclamations in the port area along the waterfront used engineered fill (Murashev and Palmer, 1998).

Two basin structures of depths greater than 100 m characterize the general structure in central Wellington and relate to the observed ground motions discussed herein. Figure 1c identifies the location of the Te Aro basin, occupying the southern area of central Wellington from the harbor edge and shallowing as it extends outward toward the surrounding hills on three sites. The Thorndon basin occupies the northern area of central Wellington, bounded on its western side by the Wellington fault that has an 80° dip (Stirling et al., 2012), resulting in a deep steep-sided valley structure in the bedrock, and extending into the harbor to the east. Previous movement of the Wellington fault resulted in uplift of the hills in the west relative to central Wellington, and as such bedrock graywacke on the western footwall side of the Wellington fault are older and less weathered than their counterpart on the eastern side for a given depth. The region to the east of the fault trace is crossed by numerous faults (van Dissen and Berryman, 1996), which will have led to greater fracturing of the bedrock in this region, and presumably resulted in lower seismic velocities. The combination of these effects suggests that there is likely an appreciable velocity contrast across the Wellington fault trace in the rock itself, in addition to that resulting from fault-bounded sediments on the hanging wall at shallow depths.

Lower Hutt-Petone is situated at the mouth of the Hutt Valley, a wedge-shaped alluvial basin ~10 km northeast of central Wellington (Fig. 1b). The Hutt Valley basin is 4.5 km

wide, 14 km long, and is bounded on its western edge by the Wellington fault that extends along the edge of the harbor from central Wellington. The valley is infilled by Quaternary alluvial-deltaic-marginal marine sediments with a maximum inferred thickness of 350 m beneath Petone, with these deposits sitting above graywacke basement rock (Boon *et al.*, 2010). The focus of this study is the site characteristics across the mouth of the Hutt Valley, which appear to be notably simpler than the site conditions in central Wellington.

Wellington Region Strong-Motion Station Network

The Wellington region has a network of over 50 SMSs as part of GeoNet, the New Zealand national hazard monitoring system (see Data and Resources). Here, we focus on the SMSs in central Wellington and the Lower Hutt-Petone areas of the Wellington region, with properties of the SMSs in the two focus areas summarized in the Central Wellington and Lower Hutt-Petone sections. Site classification metrics for GeoNet SMS in this region are summarized by Kaiser, Van Houtte, et al. (2017); since the associated quality of these classifications is variable this study presents updated classification of the fundamental site period (T_0) at these locations. This site classification metric is important in a New Zealand context; a site period of $T_0 = 0.6$ s defines the boundary between site class C (shallow soil) and site class D (deep or soft soil) in New Zealand seismic design standard NZS1170.5 (Standards New Zealand [SNZ], 2004).

Central Wellington

Figure 1c shows the locations of the nine strong-motions stations within the ~12 km² area of central Wellington central business district (CBD) in relation to the surface geologic characteristics as defined by Semmens et al. (2010). Table 1 summarizes the site characteristics of these SMSs, with the NZS1170 site classes defined by Kaiser, Van Houtte, et al. (2017). It is noted that the CPLB station is the free-field instrument from a GeoNet building array, whereas the remaining instruments are part of the GeoNet strong-motion network (Chandramohan et al., 2017). There are only two free-field sites in this area (CPLB and WEL), and apart from TEPS which is situated on the ground surface beneath the base isolated Te Papa (Museum of New Zealand) the remainder of the SMS are attached to the concrete slab foundations of a range of different low-rise structural forms (summarized in Table 1). There are two rock sites in the Wellington CBD, POTS, and WEL, both classified as NZS1170.5 site class B. POTS is situated on the edge of the Thorndon basin adjacent to the Wellington fault, whereas WEL is located at the crest of a small hill. Because WEL is known to exhibit highfrequency site amplification (Kaiser, Van Houtte, et al., 2017) influenced by topographic effects, the POTS SMS is used as the reference rock station for the central Wellington area.

Although there are five SMSs located on reclaimed deposits, these have variable characteristics in terms of

| Code | Instrument Setting | Surficial Deposits | Estimated Depth (m)* | T_0 (s) | NZS1170.5 Site Class |
|------|---------------------------------|--------------------|----------------------|-----------|----------------------|
| CPLB | Free field | Reclamation | 130 | 1.2 | D |
| FKPS | 1-story reinforced concrete | Reclamation | 60 | 0.9 | D |
| PIPS | 1-story concrete masonry | Reclamation | 250 | 1.1 | E |
| POTS | 2-story timber frame | Rock | 0 | NA | В |
| TEPS | Beneath base isolated structure | Reclamation | 120 | 1.0 | D |
| TFSS | 1-story concrete masonry | Marine deposits | 110 | 1.9 | D |
| VUWS | 1-story concrete masonry | Reclamation | 80 | 0.7 | D |
| WEL | Free field | Rock | 0 | NA | В |
| WEMS | 1-story timber frame | Alluvial deposits | 80 | 0.8 | D |

Table 1

Instrument Setting and Site Classification Metrics of Central Wellington Strong-Motion Stations

reclamation age, material, thickness, and the overall thickness of the profile above rock at these locations. PIPS is located in an area with potentially liquefiable hydraulic fill reclamation, whereas CPLB is sited above end-tipped gravel fill. FKPS reclamation consists of loose gravel fills ~8 m thick, and is in close vicinity to an old seawall. VUWS is located on some of the oldest reclamation material in the city, completed in 1875. TEPS reclamation consists of end-tipped gravel up to 13 m thick, and between this and the underlying alluvial gravels and colluvium is a soft silt layer. To improve the properties of the reclamation and silt layer, dynamic consolidation ground improvement was applied across the site in the 1990s (Murashev and Palmer, 1998). It is important to emphasize however that, for all these sites, the reclaimed deposits represent a small fraction of the overall soil profile thickness to bedrock.

The fundamental site period is used here to provide gross characterization of the local site characteristics of the soil profile at each SMS and was estimated using the horizontal-to-vertical spectral ratio method (i.e., H/V method) (Nakamura, 1989; Field *et al.*, 1990; Field and Jacob, 1993; Sánchez-Sesma *et al.*, 2011). The lowest frequency/longest period peak in the H/V spectral ratio data likely corresponds to the 1D site period for the entire soil profile down to basement rock; a significant impedance contrast, or the period of the soil profile above a strong shallow impedance contrast. The H/V method was applied here using: (1) ambient vibration records from recent field investigations and (2) a suite of earthquake-induced ground-motion records.

The ambient vibration records were collected using three-component seismometers (Nanometrics Trillium Compacts 20 s) with a flat response between 0.01 and 20 s. Thirty minutes of ambient noise were collected at each test site using a 100-Hz sampling frequency. Seismometers were leveled, oriented to magnetic north, and protected against external disturbance using a plastic cover and a sandbag. Ambient vibration records were divided into 60-s windows, and a cosine taper of 5% of the window length was used at each end of the window. Fourier spectra for the three components of motion were defined for each window/record and a Konno and Ohmachi (1998) smoothing function, with a bandwidth

coefficient of b=40 applied. The squared average of the horizontal components was computed, and the ratio between the squared average horizontal and vertical Fourier spectra for each frequency was used to define the H/V spectral ratio for each window. Here, the squared average of the horizontal Fourier spectra at each frequency f is equal to

$$H(f) = \sqrt{\frac{N^2(f) + E^2(f)}{2}},$$

in which N and E are the Fourier spectra of the north and east components of motion. Time windows that were overly noisy were removed, with the data from the remaining windows combined to develop the mean H/V data with associated uncertainty for each frequency.

Earthquake-induced ground-motion records used in the H/V method were based on those collated as part of the New Zealand Strong Motion Database (Van Houtte *et al.*, 2017). At least 10 ground-motion records were used at each site from this database, all with peak ground accelerations (PGAs) less than 0.1g. Instead of time windows, each earthquake record was processed in its entirety, with at least 10 individual earthquake records used at each SMS. These were then processed in the same manner as the ambient vibration records described previously.

Figure 2 summarizes the H/V data from six SMSs in central Wellington using both ambient and earthquakeinduced vibration data, with the mean and ± 1 standard deviation range presented by the shaded area. Azimuthal differences in the H/V data from ambient records were identified at a number of the SMS locations, potentially indicating complex subsurface features (Vantassel et al., 2018); however, this is not discussed in detail here and is a topic for further research. Table 1 summarizes the fundamental site period estimates based on the lowest frequency peaks in the H/V data. In general, there was good agreement between the H/V peaks from both the ambient and the earthquake-induced vibration data. However, assessment of the H/V data using the SESAME European Project (2004) criteria showed that the earthquake-induced vibration data did not meet clarity and reliability criteria at TFSS and VUWS. As a result, the site period estimates in Table 1 were mainly

^{*}Depths are only approximate estimates from the 3D model of Semmens et al. (2010). Standards New Zealand (SNZ, 2004).

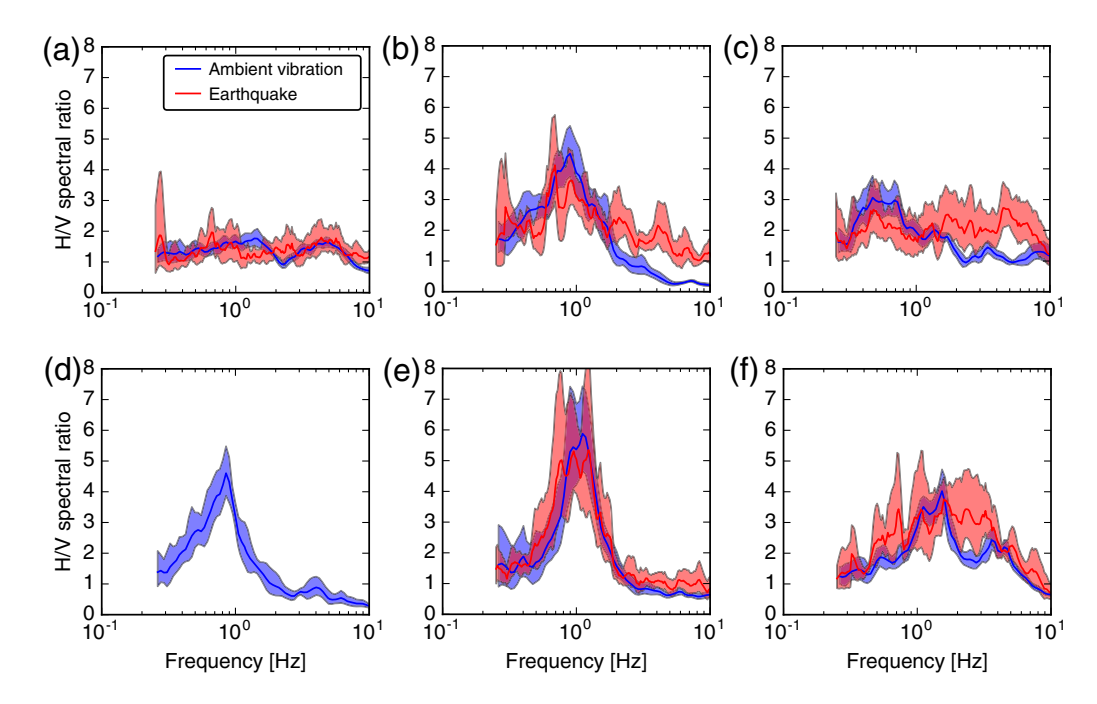


Figure 2. Horizontal-to-vertical (H/V) spectral ratio data from ambient vibration records and a suite of earthquake records at SMSs in central Wellington. Solid lines represent the mean and the shaded area indicates the ± 1 standard deviation range. (a) POTS, (b) PIPS, (c) TFSS, (d) CPLB, (e) VUWS, and (f) TEPS. The color version of this figure is available only in the electronic edition.

based on the ambient vibration data, passing the reliability criteria at all SMS but not the clarity criteria at CPLB, PIPS, TFSS, VUWS, and WEMS.

Figure 2 illustrates that POTS clearly demonstrated a flat response across the frequency range of interest, indicative of a rock site (confirmed by subsurface investigation data). PIPS had a clear peak at 0.9 Hz from the ambient data, with a peak also evident at this frequency in the earthquake data. However, there was a stronger peak at 0.7 Hz in the earthquake data, suggesting a deeper impedance contrast or a broader systematic characteristic of the earthquake records from basin-edge effects. TEPS had the clearest peak across all SMSs for both the ambient and the earthquake data at a frequency of 1 Hz. VUWS had a clear peak at 1.4 Hz in the ambient data, with a similar peak evident in the earthquake data, albeit with much higher variability. Strong azimuthal differences were evident in the ambient vibration data at TFSS. At an east-west orientation, a clear peak exists at 0.52 Hz, whereas in the north–south direction there is a clear peak at 0.7 Hz. The H/V data in Figure 2 is the squared average of the horizontal components, which represents a broader merging of these distinct peaks. The earthquake data had a peak at 0.5 Hz independent of orientation, similar to the ambient data at an east-west orientation. Only ambient data were available at CPLB, indicating a clear peak at 0.83 Hz.

Lower Hutt-Petone

In Lower Hutt-Petone, an array of SMSs is located across the mouth of the valley with variable soil profile characteristics. Figure 3 presents a schematic of this SMS array and summarizes the H/V spectral ratio data from five SMSs in the area using earthquake data. Progressing toward the east of the valley (from left to right in the figure) along the array of SMSs, the basin depth increases sharply on its western edge adjacent to the Wellington fault, before gradually reducing toward its eastern edge. The basin depth correlates well with the peaks in the H/V spectral ratios at each SMS. At PVCS and PGMS in the deeper part of the basin, the site period estimate is \sim 2.0 s. This reduces to 1.7 s at LHUS, and to 0.25 s at LIRS close to the edge of the basin. PTOS, situated just outside the basin, has a peak at \sim 0.2 s, either from the presence of shallow soil layer or as a result of topographic effects.

Ground-Motion Characteristics

Figure 4a summarizes the spatial distribution of peak vertical and geometric mean horizontal accelerations (PGAs) for the Kaikōura earthquake across central Wellington and Lower Hutt-Petone SMSs, noting that the relative distances between locations in this region is small relative to the ~60 km distance from the northern extent of the causative faults. The horizontal PGAs ranged from 0.07g to 0.24g, whereas the vertical PGAs ranged from 0.04g to 0.10g. The variation in the horizontal PGAs relates to the variability in the site characteristics across both areas discussed in the Wellington Region Strong-Motion Station Network section, with the smallest PGAs at rock sites and largest PGAs in the deepest soil deposits in both central Wellington and Lower Hutt-Petone. There is less variability in the vertical PGAs, given the reduced effect that the site characteristics have on vertical amplification.

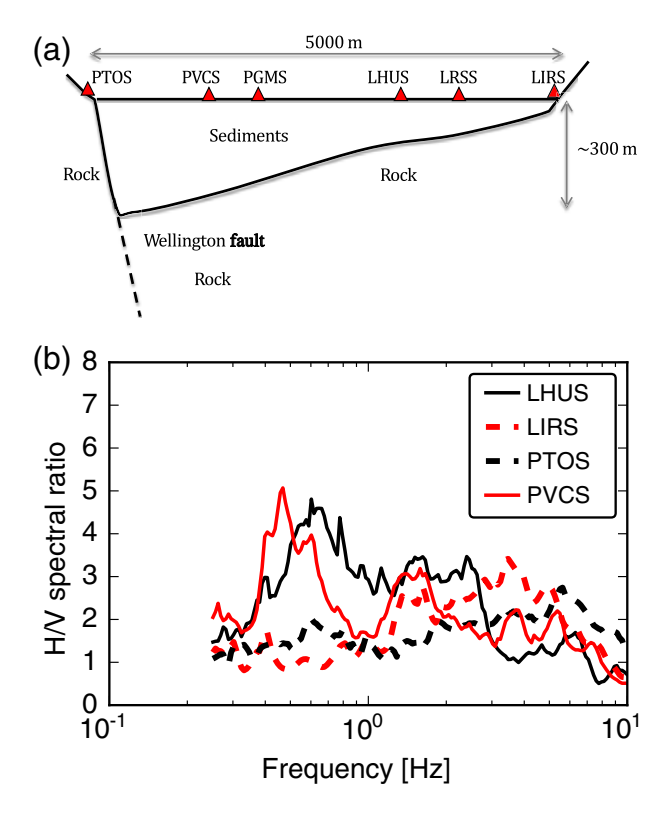


Figure 3. H/V spectral ratio data in the Lower Hutt–Petone area (a) schematic of the projected vertical cross section of the SMS locations, with vertical soil depth profile based on Boon *et al.* (2010); (b) mean earthquake record derived H/V spectral ratio data at four of these SMS locations. PGMS data are not shown as its characteristics were similar to PVCS. The color version of this figure is available only in the electronic edition.

Figure 4b provides an equivalent comparison of the spatial distribution of PGA for the 2013 Cook Strait earthquake, with a maximum horizontal PGA of 0.24g, and vertical PGA of 0.05g, similar but slightly less than the Kaikōura earthquake across all SMS locations. Ground-motion intensities were less again in the Lake Grassmere earthquake, with maximum horizontal PGAs of 0.17g in central Wellington. In all three earthquakes, the highest PGA was recorded within the Port area (stations CPLB or PIPS). In this section, a comparison of these events is used to highlight the influence of differing earthquake source and back-azimuth characteristics on the ground motions across the Wellington region.

Figure 5 compares the acceleration time series from the POTS and PIPS SMSs for the two horizontal and vertical components of motion recorded from the 2016 Kaikōura earthquake. For both SMSs, the ground motions contain two wave packets that were inferred in preliminary studies to be the result of rupture of the northern causative faults (Bradley, Razafindrakoto, and Nazer, 2017; Bradley, Razafindrakoto, and Polak, 2017; Kaiser, Balfour, et al., 2017). The influence of site effects is clearly evident in the horizontal components, with increased amplitude and lower frequency content in the PIPS site compared to the higher-frequency-dominated POTS rock site, whereas the difference between the vertical components of motion is relatively insignificant.

Central Wellington Local Site Amplification

Figure 6 presents the geometric mean acceleration response spectra for the 2016 Kaikōura earthquake, the

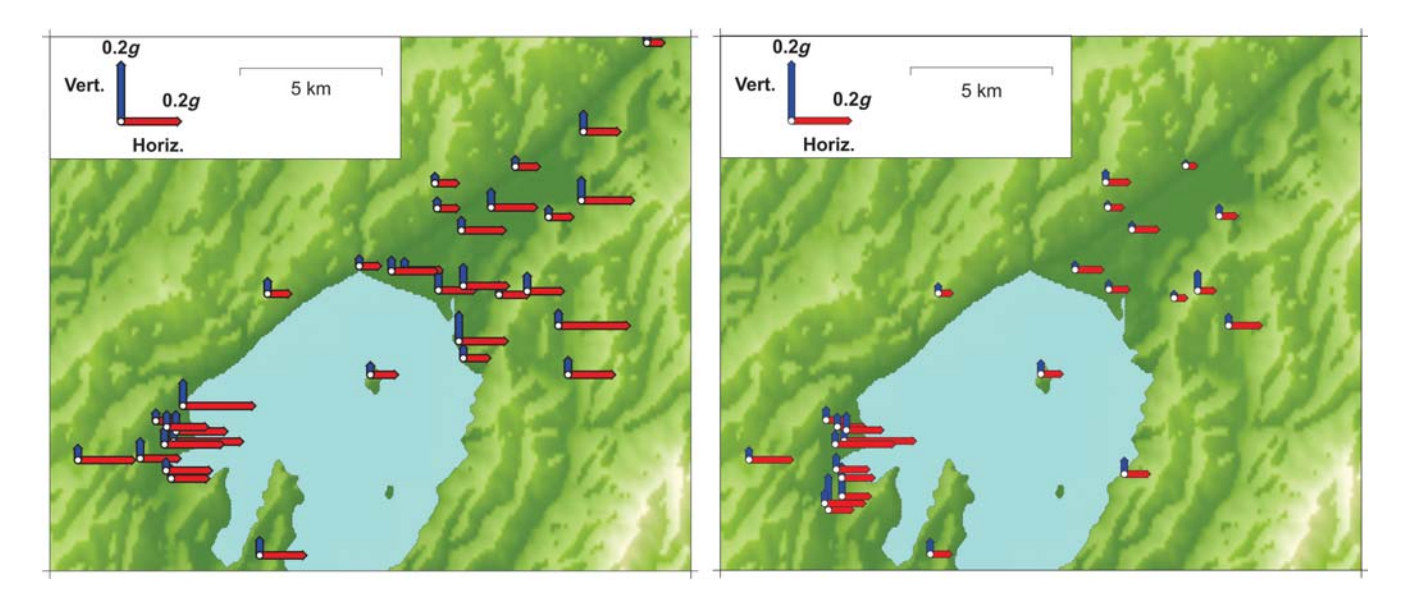


Figure 4. Horizontal (geometric mean) and vertical peak ground accelerations observed at GeoNet strong-motion stations in the central Wellington and Lower Hutt–Petone areas for the 2016 Kaikōura (left panel) and 2013 Cook Strait (right panel) earthquakes. The location of the area is indicated in Figure 1a, with the central Wellington area shown in more detail in Figure 1c. The color version of this figure is available only in the electronic edition.

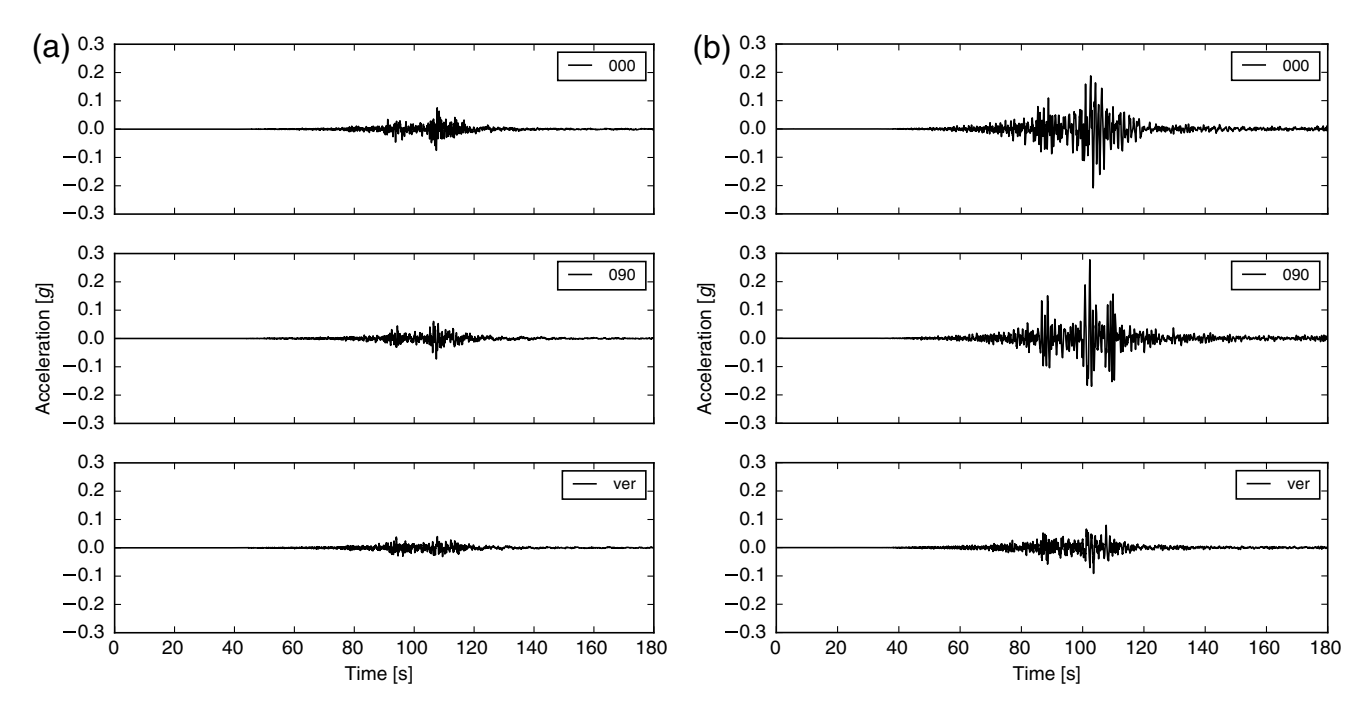


Figure 5. Acceleration time series from the (a) POTS and (b) PIPS (right) for the Kaikōura earthquake. 000, 090, and ver represent north—south, east—west, and vertical components, respectively.

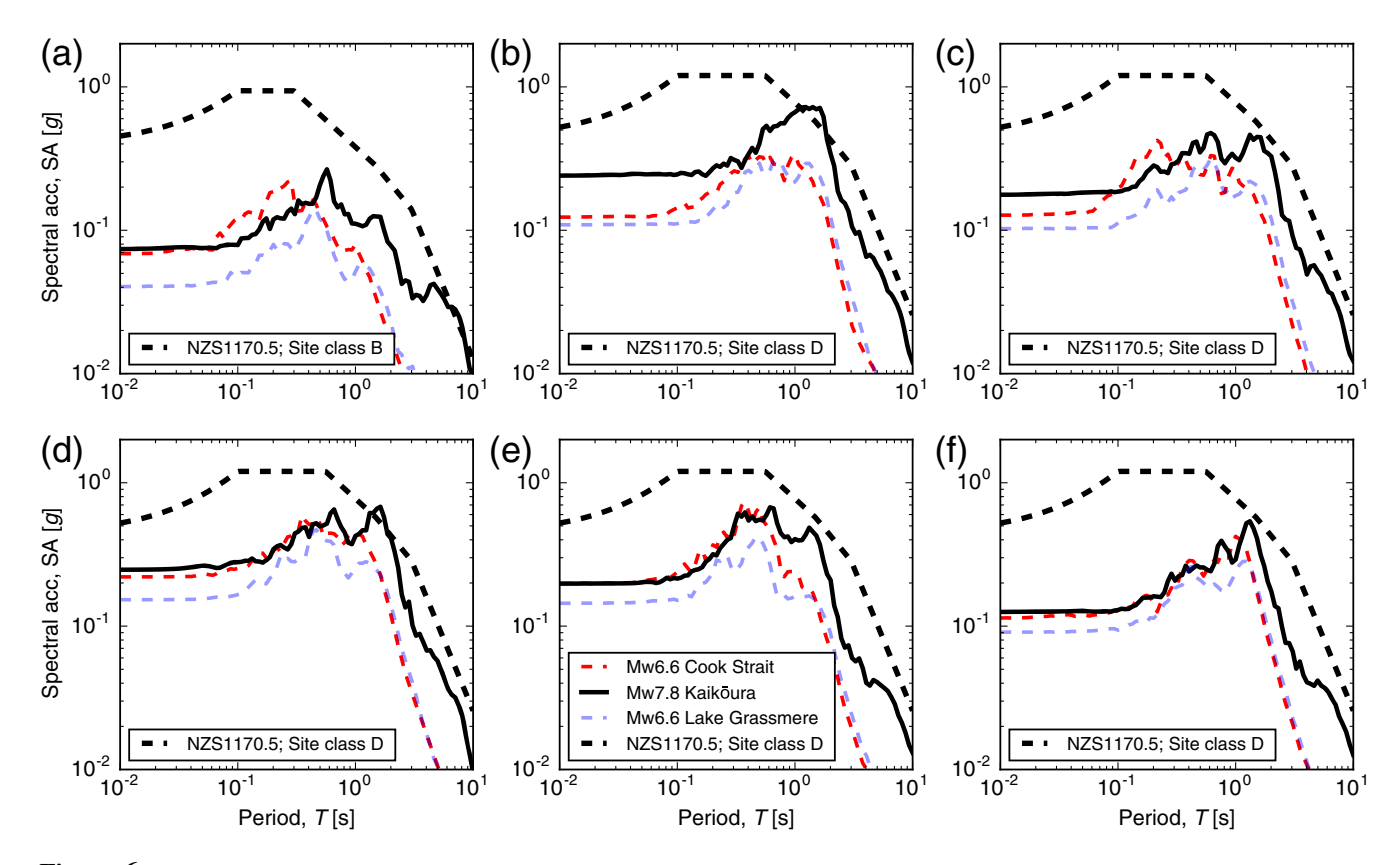


Figure 6. Observed geometric mean response spectra for SMSs in central Wellington for the 2013 Cook Strait and Lake Grassmere earthquakes and the 2016 Kaikōura earthquake. The current NZS1170.5 design spectra for the site class at each SMS are shown in each plot. (a) POTS, (b) PIPS, (c) TFSS, (d) CPLB, (e) VUWS, and (f) TEPS. The color version of this figure is available only in the electronic edition.

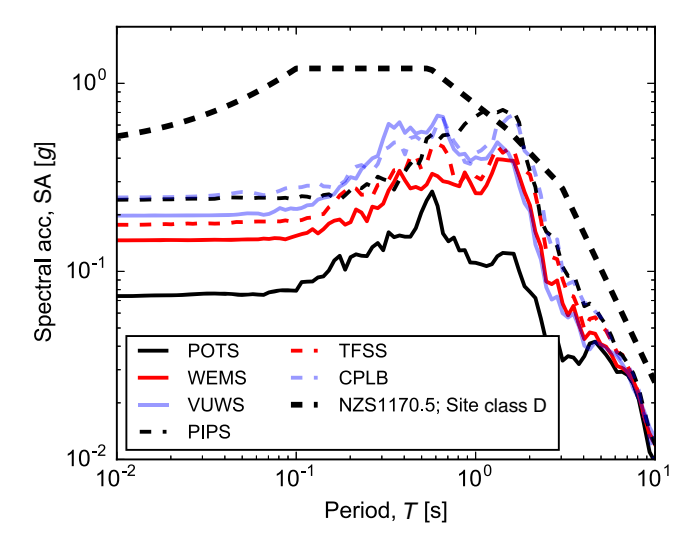


Figure 7. Observed geometric mean response spectra in central Wellington at the SMSs summarized in Figure 1c and the current NZS1170.5 site class D design spectrum for deep soil sites. The color version of this figure is available only in the electronic edition.

2013 Cook Strait earthquake, and the 2013 Lake Grassmere earthquake for six SMSs in central Wellington. These SMSs are all located within 2 km of each other, and are over 50 km from the northernmost of the causative fault ruptures. As such, these are considered to be influenced by the same source and path effects, with any differences in the spectra as a result of local site effects. The observations noted in Figure 6 and discussed herein are generally consistent with site characteristics assessed in Kaiser *et al.* (2012) and Kaiser, Van Houtte, *et al.* (2017) through prior site-response studies.

Looking across all SMSs, at short vibration periods (T < 0.6 s) spectral amplitudes for the Kaikōura and Cook Strait earthquakes are very similar, also demonstrated by the PGA characteristics in Figure 4. The most significant differences at these short periods are evident at PIPS and TFSS. The spectral amplitudes for the Lake Grassmere earthquake in this period range are the smallest at all SMS, a result of the increased distance to the causative fault for this event (compared to the Cook Strait earthquake of the same magnitude).

The spectral amplitudes increased significantly at longer periods for both rock and soil sites in Kaikōura earthquake compared to the 2013 Cook Strait and Lake Grassmere earthquakes, with the spectral amplitudes of the 2013 earthquakes very similar to each other above a vibration period of 1.5 s. At this vibration period, the difference in spectral amplitudes between the 2013 and 2016 earthquakes is approximately a factor of 2. This increased longer period spectral amplitude is the result of the larger magnitude of earthquake rupture and the associated longer duration of significant ground motions (discussed later in this article), coupled with the generally unilateral rupture of the causative faults in a general northerly direction toward Wellington (Bradley, Razafindrakoto, and Nazer, 2017; Bradley, Razafindrakoto, and Polak, 2017; Kaiser, Balfour, et al., 2017).

Figure 7 illustrates the observed ground motions in the Thorndon basin during the Kaikōura earthquake. The PIPS, CPLB, and TFSS SMSs are seen to have higher spectral amplitudes than the other SMSs for vibration periods between T=1.0 and 6.0 s, with PIPS and CPLB substantially higher between T=1.0 and 2.0 s. These have the longest estimated fundamental site periods of all the SMSs in central Wellington ($T_0=1.2$ –2.0s), and Semmens *et al.* (2010) estimated that the soil depths at the location of these SMSs, although poorly constrained in this area, are on the order of 100–250 m. The combination of deep sediments, variable depths of fill, and the location immediately beside the Wellington fault is likely to result in long-period basin-edge-generated surface waves (Kawase, 1996), which are the inferred cause of the observed long-period amplification.

Apart from PIPS during the Kaikōura earthquake, the VUWS SMS exhibited the largest spectral amplitudes at shorter vibration periods (T=0.2–1.0 s) across all SMSs and earthquakes (see also Holden *et al.*, 2013). This is likely a result of the shorter estimated fundamental period of $T_0=0.7$ s, and estimated depth to bedrock of 80 m (Semmens *et al.*, 2010) at VUWS. As described previously, VUWS also has a very thin reclamation layer and soft/loose deposits of up to 25 m thick, which could impact the observed ground motions at frequencies lower than the site period.

TEPS, the only SMS presented here from the Te Aro basin, displays a clear peak in spectral amplitude between T=1 and 2 s that is confined over a smaller period range compared to the broader spectral amplitude peaks for the SMSs in the Thorndon basin. Because this is located at a greater distance from the Wellington fault bounded edge of the Thorndon basin, the influence of basin edge-generated surface waves is not clearly evident. This is discussed in more detail in the Basin-Edge-Generated Surface Waves section of this article. The estimated fundamental site period of 1.0 s aligns well with the spectral amplitude peak for both the Cook Strait and Lake Grassmere earthquakes, and with estimations from the 1D soil profile in the vicinity of the site (Semmens et al., 2010; Kaiser et al., 2012).

Lower Hutt-Petone Local Site Amplification

Figure 8 summarizes the geometric mean horizontal acceleration response spectra from SMSs in the Hutt Valley/Petone array, providing clear illustration of site effects across an alluvial valley. The higher amplitudes at periods shorter than T=0.1 s for the soil sites are not reflective of any amplification, but a result of the peak oscillator response being driven by longer period ground motions (Bora *et al.*, 2016). The LIRS station on the eastern boundary of the valley developed mild amplification relative to the PTOS rock site on the other site of the valley, resulting from the shallow soil profile above rock at this location (with $T_0=0.25$ s). The four deeper soil sites exhibit larger amplifications over the T=0.4–4.0 s period range relative to the PTOS station,

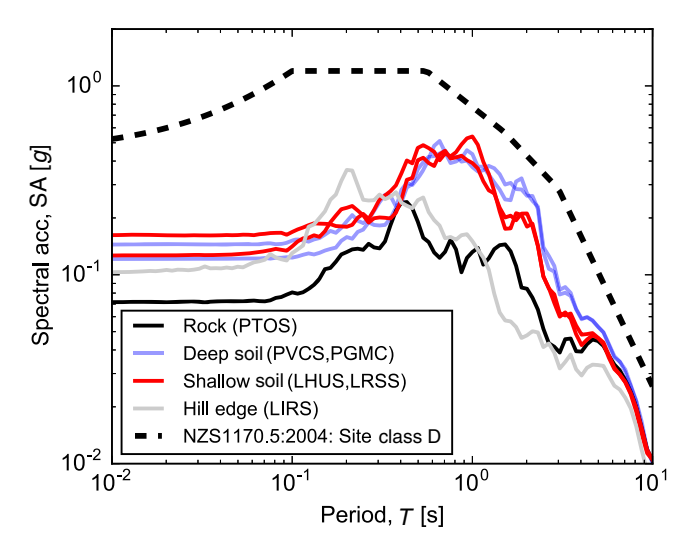


Figure 8. Observed geometric mean response spectra in the Lower Hutt–Petone area at the SMSs summarized in Figure 3 and the current NZS1170.5 site class D design spectrum for deep soil sites. The color version of this figure is available only in the electronic edition.

similar to the rock–soil site comparisons in central Wellington. There is a greater amplification for the western SMSs (PVCS and PGMS) over the T=1.5–5.0 s period range compared to the shallower SMSs to the east (LHUS and LRSS). Here, the largest difference between these two sets of SMSs occurs at \sim 2 s, corresponding to the site period of the deeper SMSs.

Significant Duration of Observed Motions

There are various metrics that can be used to describe strong-motion duration. Here, the 5%-95% significant duration D_{s595} is adopted (Bommer and Martinez-Pereira, 1999). Significant duration has the benefit of being largely independent of ground-motion amplitude, and thus provides a measure that is approximately independent of spectral acceleration amplitude. Figure 9 shows that the observed strong motions for the Kaikōura earthquake vary between approximately $D_{\rm s595} = 25$ and 30 s across the SMSs in central Wellington. There is little dependence on the nature of the site conditions, with the $D_{\rm 8595}$ for the POTS rock SMS within the range of the $D_{\rm s595}$ of the soil SMSs in the area. Figure 9 also shows that the 5%-95% significant duration of the 2013 Cook Strait ground motions was $D_{5595} = 10-11$ s, again with little dependence on the site conditions. This shorter duration combined with the lower spectral accelerations explains the reduced severity of mid-rise building stock damage experienced during this event.

The median and standard deviation range of $D_{\rm s595}$ for the Kaikōura and Cook Strait earthquakes using the empirical ground-motion models of Afshari and Stewart (2016; hereafter, AS16) and Bommer *et al.* (2009; hereafter, B09) are also presented in Figure 9. For both empirical models and events, the average source-to-site distance and generic soil

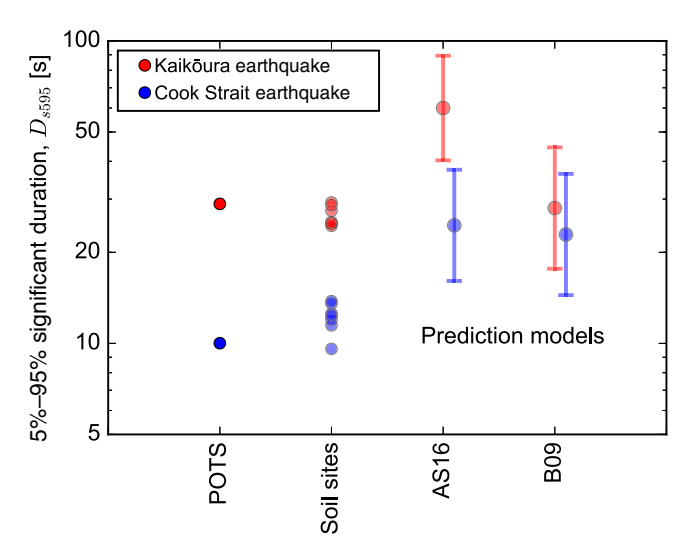


Figure 9. Comparison of 5%–95% significant duration at the central Wellington SMSs for the Kaikōura and Cook Strait earthquakes, and the median ± 1 standard deviation prediction for both earthquakes from the empirical models of Afshari and Stewart (2016; AS16) and Bommer *et al.* (2009; B09) for both events. The color version of this figure is available only in the electronic edition.

conditions represented by $V_{S30} = 250 \text{ m/s}$ were adopted because the prediction is weakly dependent on R_{rup} and V_{S30} within reasonable ranges, as seen in the observations discussed above. Figure 9 illustrates that the observed ground motions in the Kaikoura earthquake are similar to the median of the B09 model, and below the 16th percentile of the AS16 model. The observed significant durations in the Cook Strait earthquake are below the 16th percentile for both models. The B09 model exhibits very weak magnitude scaling, as seen by the similar predicted distributions for the two earthquake events in comparison to the AS16 model. The observed significant durations below the 16th percentile of the (more recent) AS16 model can be partially attributed to the appreciable rupture directivity in the Kaikōura earthquake toward Wellington (Bradley, Razafindrakoto, and Polak, 2017). Therefore, although the ground motions in Wellington during the Kaikōura earthquake were long, relative to past earthquakes affecting the region (i.e., Cook Strait), they are actually lower than predicted empirically.

Basin-Edge-Generated Surface Waves

Significant basin-edge-generated surface waves have been clearly documented in past earthquakes, for example, in the 1995 Kobe earthquake (Kawase, 1996), in Santa Monica from the 1994 Northridge earthquake (Graves *et al.*, 1998), and in Seattle from the 2001 Nisqually earthquake (Frankel *et al.*, 2002, 2009). In the Wellington region, these effects have been previously examined using small amplitude ground motions in the Lower Hutt area (Adams *et al.*, 2003) and in central Wellington from Wellington fault rupture simulations (Benites and Olsen, 2005). The distance of the

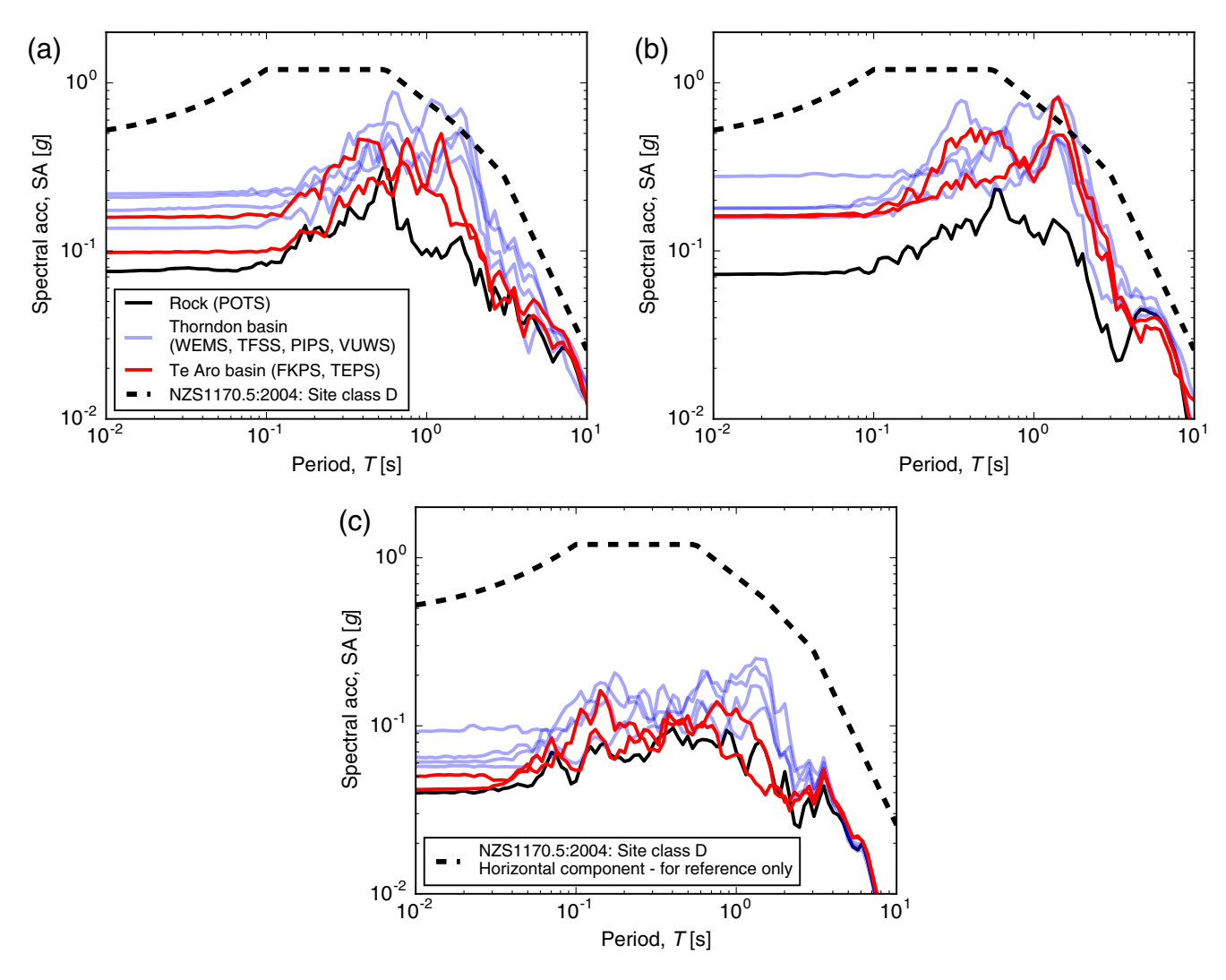


Figure 10. Comparison of the acceleration response spectra in three orthogonal components for the Kaikōura earthquake for SMSs in the two central Wellington basins and the POTS rock reference site (a) north–south, (b) east–west, and (c) vertical. NZS1170.5 site class D design spectrum is shown for comparison with the soil sites. The color version of this figure is available only in the electronic edition.

causative faults in central Wellington for the Kaikōura earthquake provides an analogous case to Santa Monica during the Northridge earthquake.

Figure 10 presents the acceleration response spectra during the 2016 Kaikōura earthquake of the SMSs located in central Wellington separated into their north–south, east—west, and vertical components. As documented via observations and 2D analyses, Graves *et al.* (1998) illustrate that basin-edge waves are most significant in the vertical direction and horizontal direction tangential to the basin edge. Each SMS has also been grouped according to their location in either the Thorndon basin, the Te Aro basin, or the POTS rock SMS (basins and locations summarized in Fig. 1c).

As discussed in the Central Wellington Local Site Amplification section, significant site amplifications occurred at the seven soil sites in both horizontal directions when compared against the POTS rock SMS. Figure 10a separates these effects further, indicating the consistently larger amplifications in the north–south component for the Thorndon basin SMSs

relative to those in the Te Aro basin, particularly between T=1.5 and 6 s. The north–south-component ground motions in the Thorndon basin are the component closer to tangential to the north end of this basin and are directly adjacent to the strong velocity contrast across the Wellington fault that defines the basin edge. In contrast, the Te Aro basin is further from the Wellington fault and is less influenced by these effects, with the north–south component roughly perpendicular to the southern edge of this basin where this strong lateral subsurface velocity contrast is not present. Figure 10b shows no clear difference in the east–west component for the SMSs in these two basins, oriented roughly parallel the Wellington fault in the Thorndon basin and perpendicular to eastern and western edges of the Te Aro basin where there is again no strong lateral subsurface velocity contrast at the basin edge.

The differences in the vertical spectral amplitudes illustrated in Figure 10c are of particular interest, as all central Wellington sites can be considered to be subject to the same underlying ground motion as a result of source and path

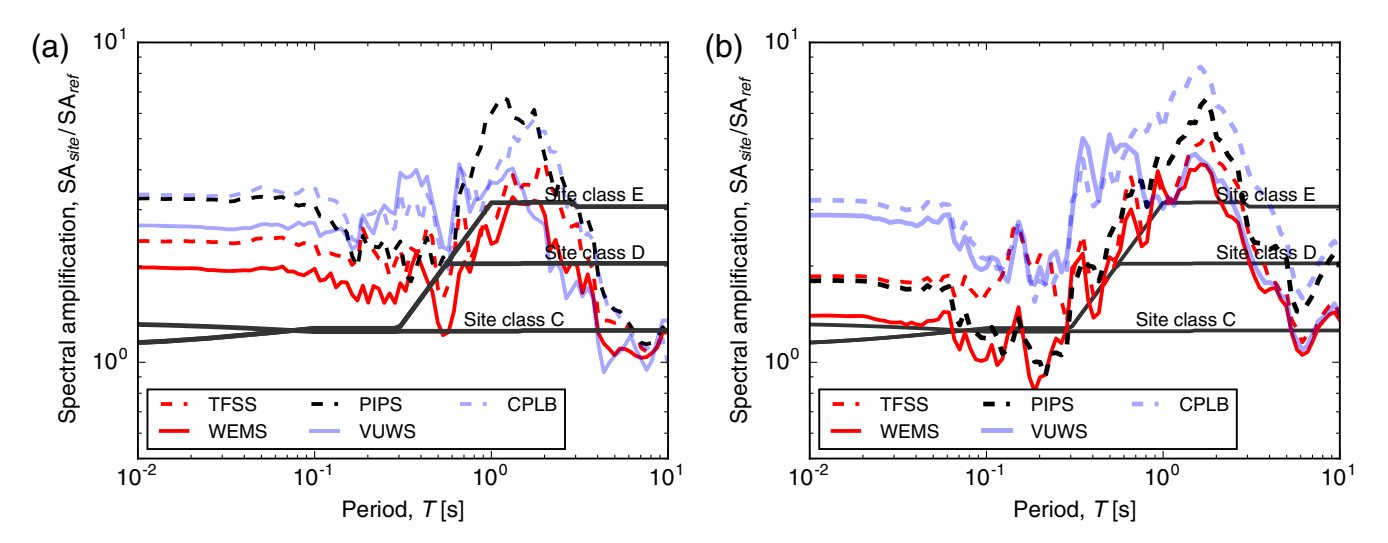


Figure 11. Spectral amplifications of the soil SMSs in the Thorndon basin with respect to the POTS rock reference SMS for the (a) Kai-kōura earthquake and (b) Cook Strait earthquake. The NZS1170.5 site amplification factors are presented in each figure, equal to the ratio of the soil site spectral shape (site classes C, D, and E) and the rock site spectral shape (site class B). The color version of this figure is available only in the electronic edition.

effects. At all SMSs in central Wellington, a shallow water table is present, and as such the *P*-wave velocity variation within the soil profile is very mild, resulting in little site amplification for vertical *P*-wave propagation. This is the case for the two SMSs in the Te Aro basin, where the vertical acceleration spectra are similar to the POTS rock SMS.

However, all sites in the Thorndon basin exhibit appreciable vertical spectral amplifications compared to the Te Aro and POTS SMS, particularly for periods in the $T=1-2~\rm s$ range. An explanation for these observations is basin-edgegenerated Rayleigh waves (which have a component of motion in the vertical direction) which occur as a result of the fault-bounded nature of the basin from the Wellington fault, or the more gradual thickening of the basin in the orthogonal northeast direction (Love waves are also generated, although not with the same amplitude, and do not have a vertical component, making them harder to distinguish in horizontal motion from direct S waves).

Because such basin-edge effects are geometrical- and impedance-driven (Kawase, 1996), they can be expected for all events in the future, although the specific character of such effects will be influenced by specifics of the earthquake source and back azimuth. Figure 6 provides some evidence of these effects during both the 2013 Cook Strait and Lake Grassmere earthquakes. At present, detailed quantification of the effect of basin-edge-generated surface waves in the Thorndon basin beyond the observational evidence above is uncertain due to the lack of data in relation to the basin characteristics. Improved characterization of the geotechnical and geophysical properties of the soil and rock units are needed to accurately assess these effects, as well as better constraint of the secondary fault structures in the area (van Dissen and Berryman, 1996) and their influence on horizontal velocity variations. We note that Benites and Olsen (2005) also highlighted the importance of basin resonance effects, particularly in the port area in a study using a coarse-scale basin-wide velocity model.

Spectral Amplification Compared to the New Zealand Code

The amplitude, frequency content, and duration characteristics of earthquake-induced ground motions are a function of the earthquake source, path, and site effects. Bradley, Razafindrakoto, and Nazer (2017) examine the consistency (or lack thereof) of the source and path effects with prediction models for the Kaikōura earthquake, whereas here we focus on a comparison of the observed site amplification at the soil SMSs in central Wellington (as summarized in Table 1) with respect to the POTS rock SMS. Observed site amplifications are compared with the NZS1170.5 (SNZ, 2004) site factors for each soil site class (C, D, and E), equal to the ratio of the soil site spectral shape and the rock site class (B) spectral shape.

Figure 11 compares the site amplification of the observed ground motions in central Wellington based on their spectral amplitude ratios with respect to the POTS reference station for the Kaikōura and Cook Strait earthquakes, with the NZS1170.5 site factors presented alongside each. Site class C soil conditions in the design standard are modeled by a site amplification of \sim 1.25 across all vibration periods, whereas site classes D and E have amplifications of \sim 2 and 3.15 at long periods, which transition back to the site class C amplification for T=0.3 s. It is noted that the NZS1170.5 site amplification factors are average factors independent of any parameters other than vibration period (i.e., they are independent of ground-motion intensity).

In the vicinity of the predominant periods of the site amplification (i.e., T = 1-2 s) the observed amplifications

for the Kaikōura earthquake significantly exceed the codebased prescriptions across all SMSs. TFSS and VUWS, which are site class D sites, have peak amplifications up to 4, as compared to the code-based maximum amplification of 2.0, whereas CPLB and PIPS amplifications are \sim 6–7, significantly greater than the maximum site class E amplification of 3.15. Overall, the Cook Strait earthquake site amplification is strongly similar to the Kaikōura earthquake, with even larger observed amplifications in the T=1–2 s range across most of the SMSs (up to a maximum of 8.5 for CPLB).

For long periods, T > 4 s, the observed spectral amplifications are ~1.0 because this is well beyond the natural vibration periods of the sites, a characteristic evident for both the Kaikōura and the Cook Strait earthquakes. This does not match the assumption of constant amplification at long periods currently being used in the code-based prescriptions. For the Kaikōura earthquake, the short period (T < 0.3 s) spectral amplifications exceed the code-based amplification of \sim 1.25, which is largely consistent across all site classes. This is to be expected for this event, because the large source-to-site distance led to a lack of nonlinearity in the site response, which would reduce this short-period amplification (this amplification is expected to be less for the type of earthquakes that dominate the Wellington hazard spectrum, i.e., in close proximity to the region). For the Cook Strait earthquake, spectral amplifications are less than the codebased values for two of the SMSs (deep profile at PIPS, and shallower profile at WEMS), and characteristics similar to the Kaikōura earthquake for TFSS, CPLB, and VUWS (again with a range of soil profile thicknesses).

The generalized code-based spectral amplifications inevitably result from the grouping, and subsequent averaging, of a large number of different soil deposits, each with their own narrowband amplifications over different vibration period ranges. Such amplification and its predominant period are also a function of the severity of the underlying rock ground-motion intensity, which the code-based factors do not explicitly consider. Differences between the two earthquakes provide some reflection of the influence of source and path effects on site response based on response spectral ratios, but these differences can be seen to be small relative to the difference in the NZS1170.5 site factor for site class D sites. Although different earthquake ruptures may induce different site effects as a result of the extent of nonlinear site response (among other factors), the presence of site/basin effects can be considered to be generally repeatable and expected in future earthquakes.

Conclusions

This article examined the characteristics of the observed ground motions in the Wellington region and the influence of site effects for the $M_{\rm w}$ 7.8 Kaikōura earthquake. At short vibrational periods, ground motions were of moderate amplitude as a result of the large distance to the causative faults of

this earthquake. However, because of site and basin-edge effects, spectral accelerations were similar to, and in some locations, exceeded the current 500-yr return-period design ground-motion levels at vibrational periods between T=1 and 2 s. The 5%–95% significant duration of ground motions in central Wellington was on the order of 30 s, consistent with empirical models for this earthquake magnitude and source-to-site distance.

Comparisons of acceleration response spectra with updated estimates of fundamental site period across central Wellington indicate that this long-period amplification is not due to 1D site effects alone, and is inferred to result from appreciable basin-edge-generated surface waves. Strong evidence for these effects is observed in particular within the Thorndon basin, although large long-period ground motions were also observed in the Te Aro basin. These long-period amplification effects have also been observed during the 2013 Cook Strait earthquake sequence, and were in some cases larger than those observed in the Kaikōura earthquake. This demonstrates that such site amplifications are repeatable for different earthquakes that produce similar levels of underlying rock ground-motion intensity.

In the Lower Hutt-Petone area at the mouth of the Hutt Valley, ground motions from the GeoNet SMS array across the wedge-shaped alluvial basin clearly demonstrated the influence of 1D site effects, with amplification effects shown to align with the estimates of the fundamental site period. All soil sites exhibited amplifications compared to rock, with the greatest amplifications at the SMSs with the longest estimated site period (as an indicator of depth).

Across the Wellington region, the large variation in site response for SMSs with the same site classification illustrates the large variation in seismic demands that would be imposed on structures built on these sites based on the same loading conditions. This suggests the need for improved formulations in design prescriptions given that such variations can be logically explained based on known geological and geotechnical conditions. These observations have also highlighted the need to improve characterization of the regional basin structures, particularly in regard to quantifying the contribution of basin resonance and basin-edge-generated surface waves.

Data and Resources

Seismograms used in this study were acquired from the GeoNet's New Zealand Strong Motion Station Database (Van Houtte *et al.*, 2017). The database can be accessed by ftp://ftp.geonet.org.nz/strong/processed/Proc/nzsmd (last accessed September 2017). Up-to-date summary of key metadata for each strong-motion station (Kaiser, Van Houtte, *et al.*, 2017) can be accessed through https://www.geonet.org.nz/data/supplementary/nzsmdb (last accessed October 2017). Figures 1a,b and 4 were created using Generic Mapping Tools v.4.5 (http://gmt.soest.hawaii.edu/, last accessed January 2018). Figure 1c was created using QGIS (https://www.qgis.org/, last accessed January 2018). All other figures were

created using Matplotlib (https://matplotlib.org, last accessed January 2018).

Acknowledgments

This research has been supported by QuakeCoRE, a New Zealand Tertiary Education Commission-funded Centre, the Royal Society of New Zealand Rutherford Discovery Fellowship Scheme, GNS Science Strategic Science Investment Fund (SSIF), the New Zealand Natural Hazards Research Platform, and the U.S. National Science Foundation (NSF) Grant CMMI-1724915. Any opinions, findings, and conclusions or recommendations expressed in this material are those of the authors and do not necessarily reflect the views of the NSF. This is QuakeCoRE Publication Number 0217. The authors acknowledge the New Zealand GeoNet project and its sponsors New Zealand Earthquake Commission (EQC), GNS Science, and Land Information New Zealand (LINZ), for providing groundmotion records used in this publication. Finally, the authors thank the two anonymous reviewers and the editors for their valuable comments and suggestions to improve the quality of the article.

References

- Adams, B. M., N. M. Osborne, and J. J. Taber (2003). The basin-edge effect from weak ground motions across the fault-bounded edge of the Lower Hutt Valley, New Zealand, *Bull. Seismol. Soc. Am.* 93, no. 6, 2703–2716, doi: 10.1785/0120010277.
- Afshari, K., and J. P. Stewart (2016). Physically parameterized prediction equations for significant duration in active crustal regions, *Earthq. Spectra* **32**, no. 4, 2057–2081.
- Baird, A., and H. Ferner (2017). Damage to non-structural elements in the 2016 Kaikōura earthquake, *Bull. New Zeal. Soc. Earthq. Eng.* 50, no. 2, 187–193.
- Begg, J. G., and C. Mazengarb (1996). Geology of the Wellington Area, scale 1:50,000, Institute of Geological & Nuclear Sciences Limited, Lower Hutt, New Zealand.
- Benites, R., and K. B. Olsen (2005). Modeling strong ground motion in the Wellington Metropolitan area, New Zealand, *Bull. Seismol. Soc. Am.* **95**, no. 6, 2180–2196, doi: 10.1785/0120040223.
- Bommer, J., and A. Martinez-Pereira (1999). The effective duration of earthquake strong motion, *J. Earthq. Eng.* **3**, no. 2, 127–172.
- Bommer, J. J., P. J. Stafford, and J. E. Alarcon (2009). Empirical equations for the prediction of the significant, bracketed, and uniform duration of earthquake ground motion, *Bull. Seismol. Soc. Am.* **99**, no. 6, 3217–3233, doi: 10.1785/0120080298.
- Boon, D., N. D. Perrin, G. Dellow, and B. Lukovic (2010). It's our fault— Geological and geotechnical characterisation and site class revision of the Lower Hutt Valley, GNS Science Consultancy Report 2010/163, 68 pp.
- Bora, S. S., F. Scherbaum, N. Kuehn, and P. J. Stafford (2016). On the relationship between Fourier and response spectra: Implications for the adjustment of empirical ground-motion prediction equations (GMPEs), *Bull. Seismol. Soc. Am.* 106, no. 3, 1235–1253.
- Bradley, B. A., H. N. T. Razafindrakoto, and M. A. Nazer (2017). Strong ground motion observations of engineering interest from the 14 November 2016 $M_{\rm w}$ 7.8 Kaikōura, New Zealand earthquake, *Bull. New Zeal. Soc. Earthq. Eng.* **50**, no. 2, 85–93.
- Bradley, B. A., H. N. T. Razafindrakoto, and V. Polak (2017). Ground motion observations from the 14 November 2016 $M_{\rm w}$ 7.8 Kaikōura, New Zealand, earthquake and insights from broadband simulations, *Seismol. Res. Lett.* **88**, no. 3, 740–756.
- Brunsdon, D., K. J. Elwood, and J. Hare (2017). Engineering assessment processes for Wellington buildings following the November 2016 Kaikōura earthquakes, *Bull. New Zeal. Soc. Earthq. Eng.* **50**, no. 2, 338–342.
- Chandramohan, R., Q. Ma, L. M. Wotherspoon, B. A. Bradley, M. Nayyerloo, S. R. Uma, and M. T. Stephens (2017). Response of instrumented buildings under the 2016 Kaikōura earthquake, *Bull. New Zeal. Soc. Earthq. Eng.* 50, no. 2, 237–252.

- Cubrinovski, M., J. D. Bray, C. de la Torre, M. J. Olsen, B. A. Bradley, G. Chiaro, E. Stocks, and L. Wotherspoon (2017). Liquefaction effects and associated damages observed at the Wellington Centreport from the 2016 Kaikōura earthquake, *Bull. New Zeal. Soc. Earthq. Eng.* 50, no. 2, 152–173.
- Field, E., and K. Jacob (1993). The theoretical response of sedimentary layers to ambient seismic noise, *Geophys. Res. Lett.* 20, no. 24, 2925–2928.
- Field, E. H., S. E. Hough, and K. H. Jacob (1990). Using microtremors to assess potential earthquake site response: A case study in Flushing Meadows, New York City, Bull. Seismol. Soc. Am. 80, no. 6, 1456–1480.
- Frankel, A., D. L. Carver, and R. A. Williams (2002). Nonlinear and linear site response and basin effects in Seattle from the M 6.8 Nisqually, Washington, earthquake, *Bull. Seismol. Soc. Am.* 92, no. 6, 2090–2109.
- Frankel, A., W. Stephenson, and D. L. Carver (2009). Sedimentary basin effects in Seattle, Washington: Ground-motion observations and 3D simulations, *Bull. Seismol. Soc. Am.* 99, no. 3, 1579–1611.
- Graves, R. W., A. Pitarka, and P. G. Somerville (1998). Ground motion amplification in the Santa Monica area: Effects of shallow basin-edge structure, *Bull. Seismol. Soc. Am.* 88, no. 5, 1224–1242.
- Hamling, I. J., S. Hreinsdóttir, K. Clark, J. Elliott, C. Liang, C. Fielding, N. Litchfield, P. Villamor, L. Wallace, T. J. Wright, *et al.* (2017). Complex multifault rupture during the 2016 $M_{\rm w}$ 7.8 Kaikōura earthquake, New Zealand, *Science* **356**, doi: 10.1126/science.aam7194.
- Henry, R. S., D. Dizhur, K. J. Elwood, J. Hare, and D. Brunsdon (2017). Damage to concrete buildings with precast floors during the 2016 Kaikōura earthquake, *Bull. New Zeal. Soc. Earthq. Eng.* 50, no. 2, 174–186.
- Holden, C., A. Kaiser, R. Van Dissen, and R. Jury (2013). Sources, ground motion and structural response characteristics in Wellington of the 2013 Cook Strait earthquakes, *Bull. New Zeal. Soc. Earthq. Eng.* 46, no. 4, 188–195.
- Kaiser, A., N. Balfour, B. Fry, C. Holden, N. Litchfield, M. Gerstenberger, E. D'Anastasio, N. Horspool, G. McVerry, J. Ristau, et al. (2017). The 2016 Kaikōura, New Zealand, earthquake: Preliminary seismological report, Seismol. Res. Lett. 88, no. 3, 727–739, doi: 10.1785/0220170018.
- Kaiser, A., C. Holden, J. Zhao, G. McVerry, and R. Benites (2012). It's our fault: Ground motion modelling of local site effects in the Wellington region, GNS Science Consultancy Report 2012/172.
- Kaiser, A., C. Van Houtte, N. Perrin, L. Wotherspoon, and G. McVerry (2017). Site characterisation of GeoNet stations for the New Zealand strong motion database, *Bull. New Zeal. Soc. Earthq. Eng.* 50, no. 1, 39–49.
- Kawase, H. (1996). The cause of the damage belt in Kobe: The basin-edge effect, constructive interference of the direct S-wave with the basininduced diffracted/Rayleigh waves, Seismol. Res. Lett. 67, no. 5, 25–34, doi: 10.1785/gssrl.67.5.25.
- Kelly, M. (2005). Heritage Trail: Old Shoreline, Wellington City Council, Wellington, New Zealand.
- Konno, K., and T. Ohmachi (1998). Ground motion characteristics estimated from spectral ratio between horizontal and vertical components of microtremor, *Bull. Seismol. Soc. Am.* 88, no. 1, 228–241.
- Langridge, R. M., W. F. Ries, N. J. Litchfield, P. Villamor, R. J. Van Dissen, D. J. A. Barrell, M. S. Rattenbury, D. W. Heron, S. Haubrock, D. B. Townsend, et al. (2016). The New Zealand active faults database, New Zeal. J. Geol. Geophys. 59, no. 1, 86–96.
- Murashev, A., and S. Palmer (1998). Geotechnical issues associated with development on Wellington's waterfront, *IPENZ Trans.* 25, no. 1, 38–46.
- Nakamura, Y. (1989). A method for dynamic characteristics estimation of subsurface using microtremor on the ground surface, Q. Rep. Railway Tech. Res. Inst. 30, no. 1, 25–33.
- Orense, R. P., Y. Mirjafari, S. Asadi, M. Naghibi, X. Chen, O. Atlaf, and B. Asadi (2017). Ground performance in Wellington waterfront area following the 2016 Kaikōura earthquake, *Bull. New Zeal. Soc. Earthq. Eng.* **50**, no. 2, 142–151.
- Sánchez-Sesma, F. J., M. Rodríguez, U. Iturrarán-Viveros, F. Luzón, M. Campillo, L. Margerin, A. García-Jerez, M. Suarez, M. A. Santoyo, and A. Rodríguez-Castellanos (2011). A theory for microtremor H/V spectral ratio: Application for a layered medium, *Geophys. J. Int.* 186, no. 1, 221–225.

- Semmens, S., G. D. Dellow, and N. D. Perrin (2010). It's our fault—Geological and geotechnical characterisation of the Wellington Central Business District, GNS Science Consultancy Report 2010/176, 52 pp.
- SESAME European Project (2004). Guidelines for the Implementation of the H/V Spectral Ratio Technique on Ambient Vibrations: Measurements, Processing and Interpretation, Deliverable D23.12.
- Standards New Zealand (SNZ) (2004). Structural Design Actions—Part 5.

 Earthquake Actions—New Zealand, NZS 1170.5:2004, Wellington, New Zealand.
- Stirling, M., G. McVerry, M. Gerstenberger, N. Litchfield, R. Van Dissen, K. Berryman, P. Barnes, L. Wallace, P. Villamor, R. Langridge, et al. (2012). National seismic hazard model for New Zealand: 2010 update, Bull. Seismol. Soc. Am. 102, no. 4, 1514–1542.
- Stirling, M. W., N. J. Litchfield, P. Villamor, R. J. Van Dissen, A. Nicol, J. Pettinga, P. Barnes, R. M. Langridge, T. Little, D. J. A. Barrell, et al. (2017). The M_w 7.8 2016 Kaikōura earthquake: Surface fault rupture and seismic hazard context, Bull. New Zeal. Soc. Earthq. Eng. 50, no. 2, 73–84.
- van Dissen, R. J., and K. R. Berryman (1996). Surface rupture earthquakes over the last c. 1000 years in the Wellington region, New Zealand, and implications for ground shaking hazard, *J. Geophys. Res.* 101, no. B3, 5999–6019.
- Van Houtte, C., S. Bannister, C. Holden, S. Bourguignon, and G. McVerry (2017). The New Zealand Strong Motion Database, *Bull. New Zeal. Soc. Earthq. Eng.* **50**, no. 1, 1–20.
- Vantassel, J., B. R. Cox, L. Wotherspoon, and A. Stolte (2018). Deep shear wave velocity profiling and fundamental site period measurements at the CentrePort, Wellington with implications for local site amplification, *Bull. Seismol. Soc. Am.* (this issue).

Department of Civil and Natural Resource Engineering
University of Canterbury
Private Bag 4800
Christchurch 8014
New Zealand
brendon.bradley@canterbury.ac.nz
(B.A.B.)

Department of Civil and Environmental Engineering University of Auckland Private Bag 92019 Auckland 1142 New Zealand (L.M.W.)

Tectonophysics Department GNS Science P.O. Box 30-369 Lower Hutt 5040 New Zealand (A.E.K.)

Department of Civil, Architectural and Environmental Engineering The University of Texas at Austin Austin, Texas 78712 (B.R.C.)

QuakeCoRE University of Canterbury Private Bag 4800 Christchurch 8014 New Zealand (S.J.)

> Manuscript received 29 September 2017; Published Online 13 March 2018; Corrected Online 14 May 2018